ISSN 1392–1320 MATERIALS SCIENCE (MEDŽIAGOTYRA). Vol. 27, No. 2. 2021

Crystallization Process, Structure and Hydrogen Absorption and Desorption Properties of Mg_xNi_{10} (x = 20.5-26.5) Alloys with Hypereutectic Composition

Xiaoping DONG [1, 2, 3] *, Yafang CHEN [1, 2], Yurui MA [1, 2], Xu LI [1, 2]

[1] *Faculty of Mechanical Design Manufacture and Automation, Hebei University, Baoding, 071002, China*
[2] *National & Local Joint Engineering Research Center of Metrology Instrument and System, Baoding, 071002, China*
[3] *Baoding New Energy Vehicle Power Engineering Technology Research Center, Baoding, 071002, China*

crossref http://dx.doi.org/10.5755/j02.ms.20926

Received 27 June 2018; accepted 31 October 2019

We have analyzed crystallization process of the Mg_xNi_{10} (x = 20.5 – 26.5) alloys using phase diagram of Mg-Ni system. Their structure, atomic arrangement and crystal defects were tested by XRD, SEM and HRTEM, respectively. Hydrogenation and dehydrogenation behaviors were measured by pressure-composition-isotherm measurement. The results show that the crystallization processes of the Mg_xNi_{10} (x = 20.5 and 22.5) alloys are unlike those of the Mg_xNi_{10} (x = 24.5 and 26.5) alloys, but their room temperature microstructure all contain Mg_2Ni and eutectic structure of Mg_2Ni + α-Mg. The alloys are composed of Mg_2Ni phase and α-Mg phase. The addition of Mg is beneficial to the formation of eutectic structure. The alloys have all good activation property. At a lower temperature, such as 200 and 250 °C, the hydrogen absorption rate and hydrogen saturation ratio are significantly lower than those of the alloy at the higher temperatures, such as 300 and 350 °C. At 350 °C, the hydrogen absorption capacity of the alloy increase and the hydrogen release efficiency of the alloy decreases with the increase of Mg content. The time of 90% of the amount of saturated hydrogen absorption and desorption of the alloys is not more than 10 and 2 minutes, respectively. The hydrogen desorption rate of the $Mg_{22.5}Ni_{10}$ alloy in the four investigated alloys is relatively large and up to 7.170 wt.%.min^{-1}.
Keywords: Mg-Ni alloy, crystallization process, structure, hydrogen absorption and desorption properties.

1. INTRODUCTION

Under enormous pressure of environmental protection, now, many countries promote environmentally friendly vehicles with low emission or zero emission. Presently, the battery electric vehicle is a matter of great concern, however, owing to technical bottlenecks including low energy density and not in a few minutes to complete the fast charging, it can not be a substitution for the traditional vehicle 100 %. Among a variety of environmentally friendly vehicles, many people are more willing to focus on hydrogen-powered cars. For it, major car companies in Japan, Korea and Europe have already completed the basic performance and development of hydrogen-powered cars, and solved many key technical problems, such as its performance, reliability, service life and environmental adaptability [1, 2]. Such as, Honda in Japan had just released clarity fuel cell vehicle from website (that is, www.battery.com.cn) in 2017, which was following TOYOTA Mirai after a production type fuel cell car on December 2014. Of course, the performance of these vehicles mainly depended on the performance of hydrogen fuel cell. In this regard, it did not start late for Chinese fuel cell, but there is a gap between the level of technology and the world first-class level. The first is the power density and service life. The former directly affects the fuel cell power system miniaturization, the latter is about 3000 hours in domestic enterprises, while the international standard is 5000 hours, and data gap is larger at home and abroad. Meantime, the key materials and components of the fuel cell are relatively weak, that is, the development of key materials including electrolyte and proton exchange membranes for fuel cells is still in the laboratory stage. These states have seriously affected the development process of China's fuel cell stack technology. Additionally, there are hydrogen storage problems. After years of research, by comparison, the reliable, effective and safe carriers of storing hydrogen energy are metal hydrides including AB5-type rare earth-based alloys, AB2-, AB3- or AB3.5-type multi-component alloys, Mg-based alloys and TiFe-based multiphase alloys. Among them, Mg hydride has displayed great expectation in the fuel cell on account of its high hydrogen storage content (7.6 wt.%) and volumetric density, reversible hydrogen absorbing performance and recyclability, etc [3, 4]. Despite all this, Mg-based hydride is still not used as the key materials of hydrogen fuel cell due to requirement of a high desorption temperature to the stored hydrogen and sluggish releasing kinetics. So, what is the minimum temperature that is easy to absorb and desorb for it? It is over 250 °C from some literature. Many researches have indicated that at high temperature, addition or replacement of the alloying elements and preparation technology could improve hydrogen absorption and desorption properties. For example, Knotek et al. [5] had study electrochemical hydriding of Mg – x wt.% Ni (x = 10.9, 14.8, 26.4 and 34.2) alloys in a 6 M KOH solution at 80 °C for 120 – 480 min, and pointed out that the Mg – 34.2 wt.% Ni alloy absorbed the highest amount of hydrogen, nearly 4.5 wt.%. De Castro et al. [6] measured the electrochemical properties of $Mg_{(55-x)}TixNi_{(45-y)}Pty$ alloys and found that $Mg_{51}Ti_4Ni_{43}Pt_2$

* Corresponding author. Tel.: +86-0312-5079330; fax: +86-0312-5079330. E-mail address: *dxp0316@163.com* (X.Dong)

composition (in at.%), which achieved 448 mAh g^{-1} of maximum discharge capacity and retained almost 66 % of this capacity after 10 cycles. In contrast, the binary $Mg_{55}Ni_{45}$ alloy achieved only 248 mAh g^{-1} and retained 11 % of this capacity after 10 cycles. Lu et al. found that maximum hydrogen storage capacity of nanocrystalline Mg and Mg – 10Ti hydride is 3.0 – 3.63 wt.% in the range of 325 – 375 °C, and dehydriding temperatures of Mg and Mg-10Ti hydride are 400 and 330 °C from TG/DTA curves, respectively [7]. Andreas et al had reported hydrogen storage experiments on MgH_2 and on ZK60 (Mg-5Zn-0.8Zr) prepared by Severe Plastic Deformation (SPD). The cold rolled MgH_2 showed a reduction of capacity by 30 % after 100 cycles, in ZK60 processed by High Pressure Torsion (HPT), both kinetics and storage capacity were stable for at least 200 absorption/desorption cycles. Although their long-term cycling is good, all hydrogenation cycles were done at a temperature of 350 °C [8]. It is reported by Lv et al. [9] that the pressure-composition isotherms (PCI) at 300 °C and the hydrogen desorption kinetics at 330 – 350 °C were measured, and the increase of Ni content decreases the hydrogen storage capacity, but the $Mg_{-x}Ni$-3La (x = 5, 10, 15, 20 at.%) alloys still kept high hydrogen storage capacity of 4.51 – 5.50 wt.%. All of the four alloys showed excellent desorption kinetics. The Mg-15Ni-3La alloy showed the highest dehydriding rate and the lowest apparent activation energy value of 80.36 kJ mol^{-1}. It had the optimum kinetics of hydrogen desorption among the alloys. The above mentioned alloying elements including Ti, Zn, Zr, La and Ni have influence on the hydrogen storage property of Mg-based alloy in varying degrees. In addition, RE (Nd, Y, Gd, Er, Sm, etc.) and transitional element (Co, Fe, Mn, Cr, Si, etc.) play similar effect [10 – 15]. From the above literatures, we can see that alloying elements have significant effects on hydrogen absorption and desorption properties of Mg based alloys. It's also worth mentioning that the hydrogen storage properties of Mg-Ni alloys with different chemical gauge rate have been studied by electrochemical method in the literature, and however, in the gaseous environment, their hydrogen absorption and desorption properties are less studied. Additionally, in the literature [5], Mg – 34.2 wt.% Ni alloy with the higher amount of hydrogen absorption was investigated, according to the Mg-Ni alloy phase diagram [16], the alloy has hypereutectic composition, and provides us with a useful information: hypereutectic Mg – Ni alloy has higher hydrogen absorption capacity under higher temperature and electrochemical condition. Take this as the model, in this paper, the absorption and desorption properties of Mg_xNi_{10} (x = 20.5 – 26.5) alloys with hypereutectic composition were investigated in a gaseous environment; furthermore, their crystallization and microstructure were also studied. The goal of this work is make readers understand the crystallization process, structure and hydrogen storage properties of the Mg-Ni alloys with hypereutectic composition, and to provide researchers with certain experimental basis and academic value.

2. EXPERIMENTAL

Ingots Mg_xNi_{10} (x = 20.5, 22.5, 24.5 and 26.5) alloys were prepared by induction melting of high purity magnesium (99.5 % purity) and nickel (99.5 % purity) loaded a Magnesia crucible in a medium frequency induction furnace filled with 40 kPa pure helium. Due to the volatilization of magnesium with low melting point of 648.8 °C, 8 % of Mg was excessively needed to compensate for the loss of Mg under the present preparation conditions. After cooling to room temperature, the ingots were pulverized by mechanical crushing until powder was not more than 300 mesh sieve. The phase structures of the powder sample were examined by a Rigaku D/max/2400 X-ray diffraction (XRD) instrument with CuKα radiation at 4 kV, 160 mA and $10°\cdot min^{-1}$. The phase abundant were calculated from the XRD data by employing Jade6.5 software and K value method (that is relative intensity ratio, abbreviation for RIR [17]), respectively. The microstructure and morphology of the as-cast alloy were characterized by a Quanta 400 type scanning electron microscopy. The hydrogenation and dehydrogenation behavior was measured by pressure-composition-isotherm (PCI) measurements at different temperatures using a Sievert's type apparatus, approximately 0.5 g powder sample was loaded into a sample holder for each test. When the vacuum is drawn for 1 hour at 400 °C, the activation properties of the alloys at 400 °C and 4.0 MPa hydrogen pressure were measured and then the hydrogenation measurement were performed under an initial hydrogen pressure in the channel of 3 MPa, dehydrogenation measurements were carried out in closed volume with beginning hydrogen pressure in the channel of 0.01 MPa and the ending until the hydrogen pressure is up to 0.03 MPa.

3. RESULTS AND DISCUSSION

3.1. Crystallization process

Fig. 1 and Fig. 2 show that phase diagram of Mg-Ni system alloy, step cooling curve and sketch map of crystallization process of the Mg_xNi_{10} (x = 20.5, 22.5, 24.5 and 26.5) alloys, respectively. According to results shown in Fig. 1 and Fig. 2, the step cooling curves of the alloys at x = 20.5 and 22.5 are on the whole the same, which apart from those of the curves of the alloys at x = 24.5 and 26.5. Here's a look at their cooling process. Firstly, $MgNi_2$ Laves phase is form through uniform reaction in the 1 – 2 point temperature range for the molten Mg_xNi_{10} (x = 20.5 and 22.5) alloys; secondly, the Mg_2Ni phase is formed between the $MgNi_2$ phase and the liquid phase through the peritectic reaction (as the reaction (1)) in the 2 – 3 point temperature range; thirdly, Mg_2Ni +α-Mg eutectic structure is formed through eutectic reaction (as the reaction (2)) at eutectic line at 506 °C. Their phase transformation process is $L \rightarrow L + MgNi_2 \rightarrow L + Mg_2Ni \rightarrow (Mg_2Ni + \alpha\text{-Mg}) + Mg_2Ni$ with the decreasing of crystallization temperature. For the molten Mg_xNi_{10} (x = 24.5 and 26.5) alloys solidification, the Mg_2Ni phase is separated out from molten alloy in the 1 – 2 point temperature range, and Mg_2Ni and α-Mg eutectic structure is form through eutectic reaction (as the reaction (2)) at eutectic line at 506 °C. Their phase transformation process is $L \rightarrow L + Mg_2Ni \rightarrow (Mg_2Ni + \alpha\text{-Mg}) + Mg_2Ni$ with the decreasing of crystallization temperature. Naturally, the room temperature microstructure of the Mg_xNi_{10} (x = 20.5 – 26.5) alloys is

composed of Mg_2Ni phase and eutectic structure of Mg_2Ni + α-Mg, and room temperature phase component contains Mg_2Ni phase and α-Mg phase.

$$L + MgNi_2 \leftrightarrows MgNi_2; \quad (1)$$

$$L \leftrightarrows Mg_2Ni + \alpha\text{-}Mg. \quad (2)$$

Now, it is necessary to apply the lever rule to calculate the relative contents of microstructure and phase, and they are listed in Table 1. Table 1 show that the more Mg content is, the greater the eutectic structure content is, the smaller the content of Mg_2Ni phase is, which indicates that the addition of Mg is beneficial to the formation of eutectic structure in our experiment. Additionally, although the composition of the alloy is in the hypereutectic region, the crystallization process and the phase transformation reaction are related to the content of Mg.

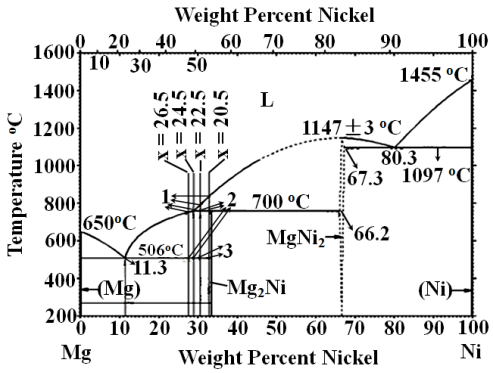

Fig. 1. Phase diagram of Mg-Ni system alloy

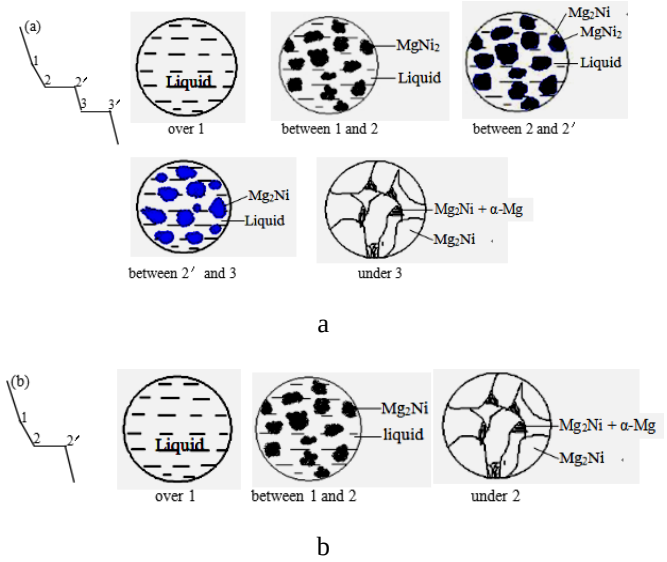

Fig. 2. Step cooling curve and sketch map of crystallization process of Mg_xNi_{10} alloy: a – x = 20.5 and 22.5; b – x = 24.5 and 26.5

3.2. Microstructure

Fig. 3 presents microscopic structural evolution of the Mg_xNi_{10} alloys. After comparing the results of different diffraction patterns of the alloys with different Mg content, the phase composition of these alloys is the same, but the intensity of the diffraction peaks is different, that is, each pattern is dominated by the peaks of hexagonal Mg_2Ni (JCPDS 35-1225; a = 0.520 nm, c = 1.3320 nm) compounds phase, and small quantity of hcp α-Mg (JCPDS 35-0821) is also presented. The present of α-Mg in Mg-Ni alloys is normal because the experimental alloy contains excess amounts of Mg compared to the Mg_2Ni stoichiometric concentrations [18]. Besides, the strongest diffraction peak intensity about Mg_2Ni phase and α-Mg phase for the alloys with x = 20.5, 22.5, 24.5 and 26.5 are 6056, 8357, 6776, 8367 and 136, 836, 1017, 1858, respectively. Using the strongest diffraction peak intensity of the Mg_2Ni phase and α-Mg phase, we have used the *K* value method [17] (that is, Relative Intensity Ratio, abbreviated as RIR, as Eq. 3) to calculate their phase abundance, in Eq. 3, *K* values of Mg_2Ni and Mg are 2.89 and 4.01 by MDI Jade6.0 software respectively.

$$W_x = \frac{I_{X\,i}}{K_A^X \sum_{i=A}^{N} \frac{I_i}{K_A^i}}, \quad (3)$$

where I_{X_i} is the strongest diffraction peak intensity of X_i phase and K_A^i is *K* value of each phase as Mg_2Ni phase of internal standard substance.

Comparing results in Table 1, there are very small differences between the phase contents calculated by the lever rule and by *K* value method from the XRD, which shows that the metallurgical effect of Mg-Ni alloy is better, and Mg volatilization was properly control during melting.

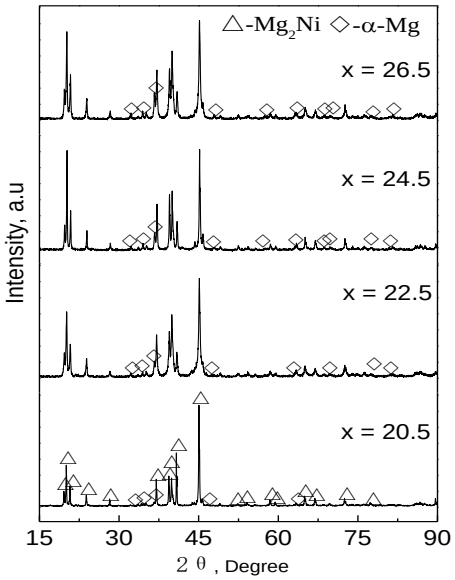

Fig. 3. XRD patterns of Mg_xNi_{10} alloys

SEM images of the Mg_xNi_{10} alloys are presented in Fig. 4. Fig. 4 show that the surface of the alloy consists of gray regions and black regions, corresponding to the Mg_2Ni phase and a very fine eutectic structure of Mg_2Ni + α-Mg, respectively. For the Mg_2Ni phase, the shape of its grain changes from fish-bone (x = 20.5) to sharp-edged polyhedral (x = 22.5 and 24.5) to long block of varying size (x = 26.5) with the increase of Mg content.

Table 1. Relative content of microstructure and phase of the alloy at room temperature

x	Content of microstructure, wt.%		Content of phase[a], wt.%		Content of phase[b], wt.%	
	eutectic	Mg_2Ni	Mg_2Ni	α-Mg	Mg_2Ni	α-Mg
20.5	1.99	98.01	98.87	1.13	98.41	1.59
22.5	9.40	90.60	94.64	5.36	93.28	6.72
24.5	16.23	83.77	90.75	9.25	90.23	9.76
26.5	22.52	77.48	87.17	12.83	86.20	13.80

Notes: [a] represents results obtained from the lever rule;
[b] represents results obtained from the XRD and *K* value method.

The formation of eutectic structure is because that the molten Mg-Ni alloy solidifies through the Mg-Ni eutectic line with the decrease of crystallization temperature in this experiment. The eutectic reaction inevitably occurs and the eutectic structure is formed [16]. As shown in Fig. 4 e of greater magnification, the Mg_2Ni and α-Mg phases are distributed in lamellar form in the fine eutectic mixture. Knotek et al. [5] had considered that that the dispersed eutectic structure with a high volume fraction form a large number of phase boundaries, which can make it available for hydrogen atom diffusion in the alloy. The above results further confirmed the results of phase diagram analysis.

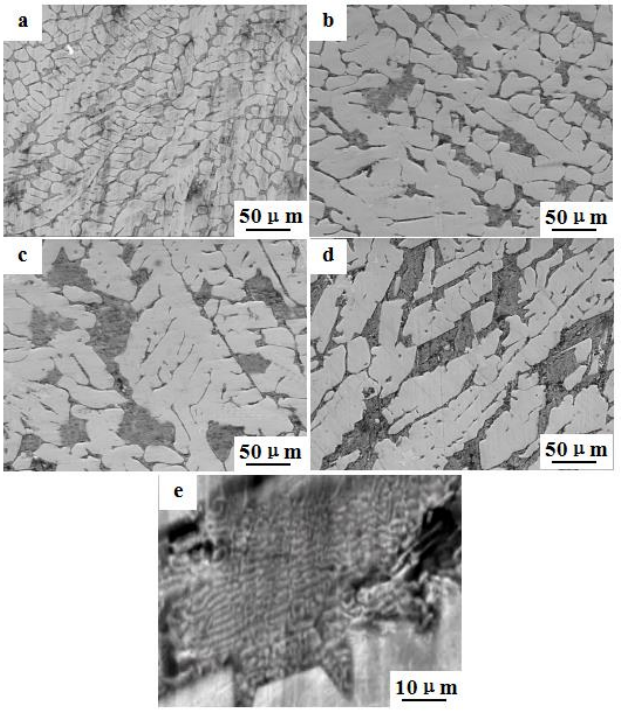

Fig. 4. SEM images of the Mg_xNi_{10} alloys: a – x = 20.5; b – x = 22.5; c – x = 24.5; d – x = 26.5; e – eutectic structure

Fig. 5 show high resolution transmission electron microscopy (HRTEM) image of the Mg_xNi_{10} alloys. The alloys have polycrystalline structure. Mg atoms and Ni atoms are arranged neatly, but there are many obvious differences in the crystal orientation and quantity owing to the different atomic arrangement. The crystal orientation and quantity in different directions increase with the increase of Mg content. The number of high-angle grain boundaries over 10° is larger. The crystal is anisotropic owing to the different atomic arrangement of the crystal faces and their upward atoms. Besides, the vacancy (as in ellipse) exists, which increase and become more and more obvious with the increase of Mg content. Remarkably, there is twin structure (as in rectangle) in the $Mg_{26.5}Ni_{10}$ alloy.

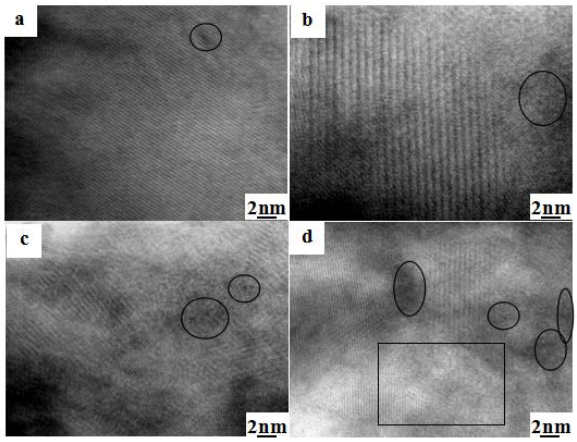

Fig. 5. HRTEM images of the Mg_xNi_{10} alloys: a – x = 20.5; b – x = 22.5; c – x = 24.5; d – x = 26.5

3.3. Activation characteristics

The activation curves of the Mg_xNi_{10} (x = 20.5 – 26.5) alloys with different Mg content at 400 °C and 4.0 MPa are compared in Fig. 6. Obviously, the alloys have all good activation properties under the favorable temperature and pressure conditions. That is to say, two or three hydrogen absorption and desorption cycles at experimental conditions are enough to activate for the Mg_xNi_{10} (x = 20.5 – 26.5) alloys. These results are related to vacancy and multiphase or polycrystalline boundary (as shown Fig. 4 and Fig. 5) in the alloy. According to the literature [19], the atomic arrangement in high angle grain boundaries (misorientation is greater than 10°) is more disordered, meantime, there are many vacancy and dislocation defects at this grain boundary. Besides, the polycrystalline/multiphase boundary interfaces provide space for the release of strain energy produced by expansion and shrinkage of the lattice during hydrogen absorption and desorption. So, these defects can provide good channel for hydrogen diffusion and migration, and accelerate the reaction of hydrogen atom and hydrogen absorbing elements. In addition, the activation properties of the $Mg_{24.5}Ni_{10}$ and $Mg_{26.5}Ni_{10}$ alloys are slightly better than those of the $Mg_{20.5}Ni_{10}$ and $Mg_{22.5}Ni_{10}$ alloys. This is because that the content of eutectic structure increase with the increase of Mg content (as shown in Table 1), the more the content is, the more grain boundary and phase boundary the fine and lamella eutectic structures in the alloys is.

It is also noteworthy from Fig. 6 that the hydrogenation curves before activation of all the alloys have a smaller slope, especially the first hydrogenation curve, which means that the first hydrogenation reactions have slow kinetics, even incomplete. Interestingly enough, the hydrogen absorption processes at activation and after activation display fast kinetics. This result is ascribed to the effect of crystal defects and the pulverization degree of alloy particle size caused by the release of internal stress produced by expansion and contraction when the hydrogen atoms enter and go out of the lattice [20], respectively.

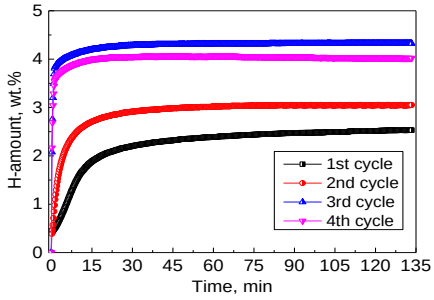

a

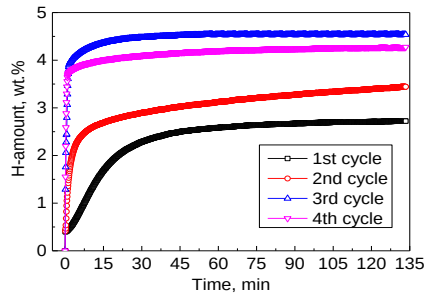

b

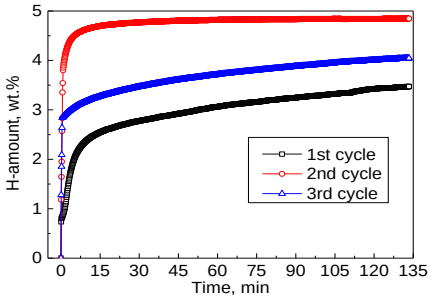

c

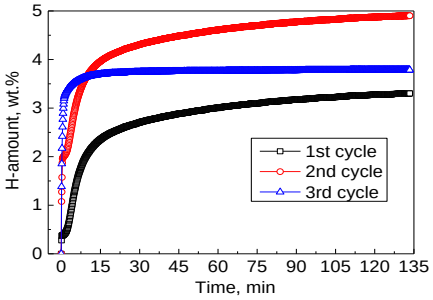

d

Fig. 6. Activation curves of the Mg_xNi_{10} alloys: a – x = 20.5; b – x = 22.5; c – x = 24.5; d – x = 26.5

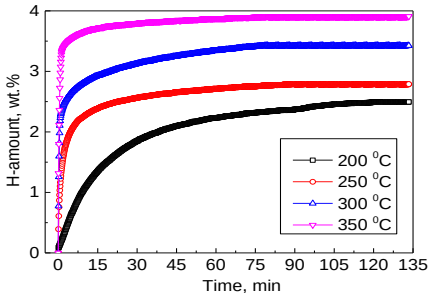

a

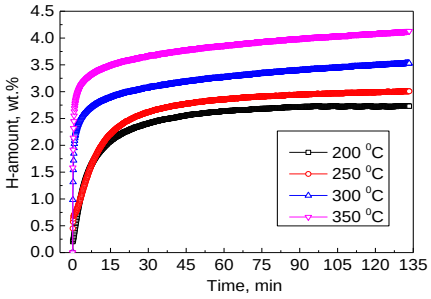

b

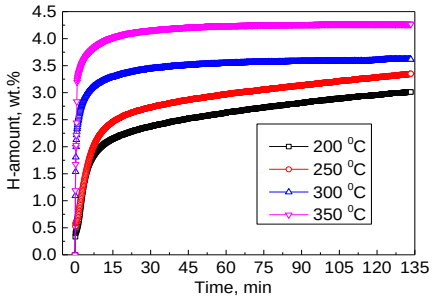

c

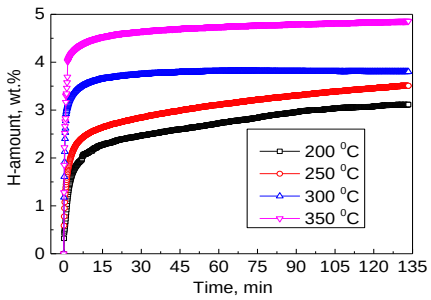

d

Fig. 7. Hydrogen absorption curves of the Mg_xNi_{10} alloys: a – x = 20.5; b – x = 22.5; c – x = 24.5; d – x = 26.5

3.4. Hydrogen absorption and desorption properties

Hydrogen absorption and desorption curves of the alloys at different test temperatures are shown in Fig. 7 and Fig. 8, respectively. For the same alloy, it is significant that the influence of temperature on hydrogen absorption and desorption properties of the alloys. At a lower temperature, such as 200 and 250 °C, the hydrogen absorption rate and hydrogen saturation ratio are significantly lower than those of the alloy at the higher temperatures, such as 300 and 350 °C. For instance, for the $Mg_{24.5}Ni_{10}$ alloy, within 8 minutes, the slope of the hydrogen absorption curve of the alloy increases with the rise of test temperature.

For the alloy hydride, the higher the test temperature is, the more the absolute value of slope of the hydrogen desorption curve of the alloy is. The average hydrogen absorption rate of the alloy is 0.235 wt.%.min^{-1}, 0.259 wt.%.min^{-1}, 0.392 wt.%.min^{-1}, 0.481 wt.%.min^{-1} at 200, 250, 300 and 350 °C within 8 minutes, respectively. However, the rate of hydrogen desorption of alloy hydride is much faster than that of hydrogen absorption. Within 1 minute, hydrogen evolution rate of the alloy hydride is 0.401 wt.%.min^{-1}, 0.897 wt.%.min^{-1}, 1.977 wt.%.min^{-1}, 3.582 wt.%.min^{-1} at 200, 250, 300 and 350 °C, respectively. The saturated hydrogen absorption and desorption capacity of the alloy is 3.013 and 1.828 wt.%, 3.351 and 2.669 wt.%, 3.615 and 3.479 wt.%, 4.269 and 3.979 wt.% at 200, 250,

300 and 350 °C, respectively. 90 % of the amount of saturated hydrogen absorption and desorption of the alloy reaches within 72.4 and 4.2 min, 67.3 and 8 min, 12.4 and 3.2 min, 7.8 and 1 min at 200, 250, 300 and 350 °C, respectively. To the same alloy, the higher temperature is favorable for improving the hydrogen absorption and desorption property of the alloy. As is known to all, the occurrence of reaction requires the two conditions of thermodynamics and kinetics [19, 20], being in relation to temperature and atomic diffusion rate, respectively. However, the two interact with each other. The atoms at lower temperature not gotten enough activation energy, which makes it difficult to diffuse, the higher the temperature is, the more favorable the diffusion of atoms is. Therefore, the hydrogen absorption and desorption reaction is relatively good at higher temperature.

How is the relationship between the hydrogen absorption/desorption property and the Mg content at the same temperature? Hydrogen absorption and desorption properties of the alloys at 350 °C are analyzed. For the hydrogen absorption/desorption curves, the alloys have faster rate of hydrogen absorption/desorption at this temperature. The saturated hydrogen absorption and desorption capacities of the alloys are 3.909 and 3.906, 4.128 and 3.969, 4.269 and 3.979, 4.858 and 3.944 wt.% for the $Mg_{20.5}Ni_{10}$, $Mg_{22.5}Ni_{10}$, $Mg_{24.5}Ni_{10}$ and $Mg_{26.5}Ni_{10}$ alloys, respectively, suggesting that the hydrogen absorption capacity increases with the increase of Mg content. Compared with the absorption of hydrogen, we found that the efficiency of hydrogen desorption, which is defined as the ratio of saturated hydrogen absorption capacity to saturated hydrogen desorption capacity, reduces with the increase of Mg content. Namely, they are 99.92 %, 96.15 %, 93.21 %, 81.19 % for the $Mg_{20.5}Ni_{10}$, $Mg_{22.5}Ni_{10}$, $Mg_{24.5}Ni_{10}$ and $Mg_{26.5}Ni_{10}$ alloys, respectively. Generally, the hydrogen absorption capacity in Mg phase is higher than that of Mg_2Ni phase. According to the above-mentioned results calculated by XRD diffraction (as shown in Fig. 3 and Table 1), it is found that Mg_2Ni phase amount decreases and α-Mg phase amount increase with the increase of Mg content. Therefore, the hydrogen absorption capacities of the alloys increase. However, reduction of hydrogen desorption efficiency with the increase of Mg content, which is because that the hydrogen desorption condition of MgH_2 is harsh. In the temperature range of this experiment, a part of hydrogen is not released [21]. The more the content of Mg is, the more obvious this phenomenon.

The time of 90 % of the amount of saturated hydrogen absorption and desorption of the $Mg_{20.5}Ni_{10}$, $Mg_{22.5}Ni_{10}$, $Mg_{24.5}Ni_{10}$ and $Mg_{26.5}Ni_{10}$ alloys needs 4.3 and 2 minutes, 9.6 and 0.7 minutes, 7.8 and 1 minutes, 7.2 and 1.3 minutes, respectively. The hydrogen absorption rates of the $Mg_{20.5}Ni_{10}$, $Mg_{22.5}Ni_{10}$, $Mg_{24.5}Ni_{10}$ and $Mg_{26.5}Ni_{10}$ alloys are 2.232 wt.%.min^{-1}, 1.928 wt.%.min^{-1}, 2.241 wt.%.min^{-1}, 2.675 wt.%.min^{-1} within 1.5 minutes, however, the hydrogen desorption rates of the alloys are very fast, namely, within 1 minute, the hydrogen desorption rates of the $Mg_{20.5}Ni_{10}$, $Mg_{22.5}Ni_{10}$, $Mg_{24.5}Ni_{10}$ and $Mg_{26.5}Ni_{10}$ alloys are 6.218 wt.%.min^{-1}, 7.170 wt.%.min^{-1}, 6.370 wt.%.min^{-1} and 5.512 wt.%.min^{-1}, respectively. From the above, we know that the time of 90% of the amount of saturated and rates hydrogen absorption and desorption show variation without law with the rise of Mg content in prophase of hydrogen absorption and desorption. Still, it can be seen from the above results that the time of reaching 90 % of the amount of saturated hydrogen absorption of the alloys is less and is not more than 10 minutes. For desorption, it is not more than 2 minutes. The alloy has the larger the hydrogen absorption and desorption rate, this mainly ascribes that fine and lamellae eutectic structure makes hydrogen atom diffusing easily, the synergistic effect of Mg phase and Mg_2Ni phase in absorbing hydrogen.

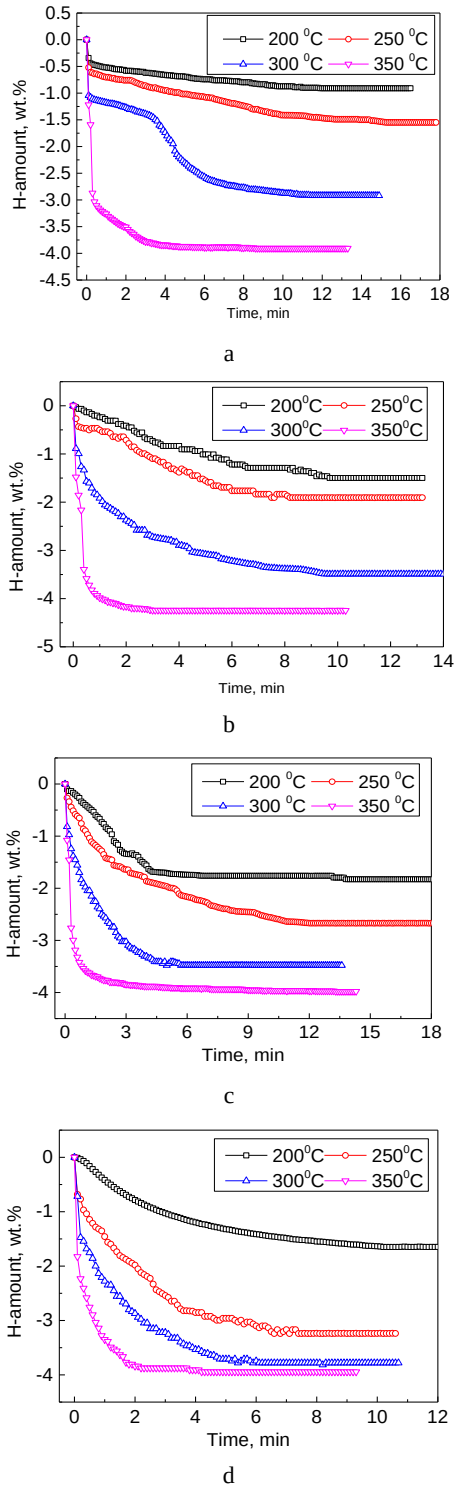

Fig. 8. Hydrogen desorption curves of the Mg_xNi_{10} alloys: a – x = 20.5; b – x = 22.5; c – x = 24.5; d – x = 26.5

4. CONCLUSIONS

Crystallization process of the Mg_xNi_{10} (x = 20.5 – 26.5) hypereutectic alloys with different Mg content is also different, the phase transformation process of the $Mg_{24.5}Ni_{10}$ and $Mg_{26.5}Ni_{10}$ alloys are $L \rightarrow L + MgNi_2 \rightarrow L + Mg_2Ni \rightarrow (Mg_2Ni + \alpha\text{-}Mg) + Mg_2Ni$, and the phase transformation process of the $Mg_{20.5}Ni_{10}$ and $Mg_{22.5}Ni_{10}$ alloys are $L \rightarrow L + Mg_2Ni \rightarrow (Mg_2Ni + \alpha\text{-}Mg) + Mg_2Ni$. Their room temperature microstructure of the alloys is composed of Mg_2Ni and a fine eutectic mixture of Mg_2Ni + α-Mg, Mg can contribute to the formation of eutectic structure. In this study, the molten Mg-Ni alloys with higher Mg content have more eutectic structure and less Mg_2Ni phase content. The diffraction peaks are dominated by the peaks of hexagonal Mg_2Ni phase and small quantity of hcp α-Mg phase. The alloys have polycrystalline structure. The crystal orientation and quantity in different directions increase with the increase of Mg content. There are anisotropic for crystal and vacancy increase with the increasing Mg content. There is twin structure (as in rectangle) in the $Mg_{26.5}Ni_{10}$ alloy.

The first hydrogenation reactions have slow kinetics, even incomplete; however, the hydrogen absorption processes at activation and after activation display fast kinetics. At a lower temperature, such as 200 and 250 °C, the hydrogen absorption rate and saturation absorption of hydrogen are significantly lower than those of the alloy at the higher temperatures, such as 300 and 350 °C. At 350 °C, the amount of hydrogen absorption and desorption of these hypereutectic alloys is over 3.9 wt.%, but, the hydrogen release efficiency of alloy decreases with the increase of Mg content.

At 350 °C, the time of 90 % of the amount of saturated hydrogen absorption and desorption of the alloys is less and is not more than 10 and 2 minutes, respectively. The hydrogen desorption rates of the $Mg_{22.5}Ni_{10}$ alloy of the four alloys is relatively large and up to 7.170 wt.%.min^{-1}.

In this study, we obtained the crystallization process, room temperature structure, phase and relative content of Mg-Ni alloy with hypereutectic composition. Meantime, good activation properties and hydrogen absorption at different test temperatures about these alloys are reflected.

Under the microstructure with eutectic microstructure, the alloy has good activation properties and high hydrogen absorption. Especially important, $Mg_{22.5}Ni_{10}$ alloy has relatively good hydrogen absorption and desorption kinetics among the four alloys studied. It provides an important experimental basis for researchers to develop alloy compositions in this direction.

Acknowledgments

This work was supported by National Natural Science Foundation of China [grant number 51371094], Natural Science Foundations in Hebei province [grant number E2018201235] and Baoding Science and Technology Plan Project (2074P019).

REFERENCES

1. **Zhang, H.W., Zheng, X.Y., Tian, X., Liu, Y., Li, X.** New Approaches for Rare Earth Magnesium Based Hydrogen Storage Alloys *Process in Natural Science: Materials International* 27 (1) 2017: pp. 50 – 57. https://doi.org/10.1016/j.pnsc.2016.12.011
2. **Wei, T.Y., Lim, K.L., Tseng, Y.S., Sli, C.** A Review on the Characterization of Hydrogen in Hydrogen Storage Materials *Renewable and Sustainable Energy Reviews* 79 2017: pp. 1122 – 1133. https://doi.org/10.1016/j.rser.2017.05.132
3. **Durbin, D.J., Malardier-Jugroot, C.** Review of Hydrogen Storage Techniques for on Board Vehicle Applications *International Journal of Hydrogen Energy* 38 (34) 2013: pp. 14595 – 14617. https://doi.org/10.1016/j.ijhydene.2013.07.058
4. **Bhattacharyya, R., Mohan, S.** Solid State Storage of Hydrogen and its Isotopes: An Engineering Overview *Renewable and Sustainable Energy Reviews* 41 (41) 2015: pp. 872 – 883. https://doi.org/10.1016/j.rser.2014.09.004
5. **Knotek, V., Vojtěch, D.** Electrochemical Hydriding of Mg-Ni-Mm (Mm = mischmetal) Alloys as an Effective Method for Hydrogen Storage *International Journal of Hydrogen Energy* 38 (37) 2013: pp. 3030 – 3040. https://doi.org/10.1016/j.ijhydene.2012.12.112
6. **de Castroa, J.F.R., Santosb, S.F., Nikkunia, F.R., Ishikawac, T.T., Ticianellia, E.A.**, Structural and Electrochemical Characteristics of $Mg_{(55-x)}Ti_xNi_{(45-y)}Pt_y$ Metal Hydride Electrodes *Journal of Alloys and Compounds* 498 (1) 2010: pp. 57 – 61. https://doi.org/10.1016/j.jallcom.2010.03.097
7. **Lu, W.C., Ou, S.F., Lin, M.H., Wong, M.F.** Hydriding Characteristics of Mg–Ti Alloys Prepared by Reactive Mechanical Grinding and Hydrogen Pulverization *Journal of Alloys and Compounds* 664 2016: pp. 193 – 198. https://doi.org/10.1016/j.jallcom.2015.12.064
8. **Andreas, G., Jelena, H., Ajit, P., Gerhard, K., Michael, Z.** Long-term Hydrogen Storage in Mg and ZK60 after Severe Plastic Deformation *International Journal of Hydrogen Energy* 40 (47) 2015: pp. 17144 – 17152. https://doi.org/10.1016/j.ijhydene.2015.05.145
9. **Lv, Y.J., Zhang, B., Wu, Y.** Effect of Ni Content on Microstructural Evolution and Hydrogen Storage Properties of Mg–xNi–3La (x=5, 10, 15, 20at.%) Alloys *Journal of Alloys and Compounds* 641 2015: pp. 176 – 180. https://doi.org/10.1016/j.jallcom.2015.04.074
10. **Xie, L.S., Li, J.S., Zhang, T.B., Kou, H.C.** De/hydrogenation Kinetics Against Air Exposure and Microstructure Evolution during Hydrogen Absorption/Desorption of Mg-Ni-Ce Alloys *Renewable Energy* 113 2017: pp. 1399 – 1407. https://doi.org/10.1016/j.renene.2017.06.102
11. **Dell'Era, A., Pasquali, M., Ciprioti, S.V., Lupim, C., Tuffim, R.** Synthesis and Characterization of a MgNi-RE Alloy for Hydrogen Storage *International Journal of Hydrogen Energy* 42 (42) 2017: pp. 26333 – 26342. https://doi.org/10.1016/j.ijhydene.2017.08.207
12. **Agarwalm, S., Jainm, A., Jainm, P., Jangirm, M., Vyasm, D., Jainam, I.P.** Effect of ZrCrCo alloy on Hydrogen Storage Properties of Mg *Journal of Alloys and Compounds* 645 (S1) 2015: pp. S518 – S523. https://doi.org/10.1016/j.jallcom.2014.12.068
13. **Zhang, Y.H., Yang, T., Shang, H.W., Zhangm, G.F., Cai, Y., Zhao, Z.L.** Gaseous and Electrochemical Hydrogen Storage Kinetics of as-Quenched Nanocrystalline and Amorphous Mg_2Ni-Type Alloys *Journal of Wuhan*

University of Technology-Materials. Science Edition 28 (3) 2013: pp. 604 – 611.
https://doi.org/10.1007/s11595-013-0738-x

14. **Manivasagam, T.G., Iliksu, M., Danilov, D.L., Notten, P.H.L.** Synthesis and Electrochemical Properties of Binary MgTi and Ternary MgTiX (X = Ni, Si) Hydrogen Storage Alloys *International Journal of Hydrogen Energy* 42 (37) 2017: pp. 23404 – 23415.
https://doi.org/10.1016/j.ijhydene.2017.03.093
15. **Wang, Y., Wang, J.** Recent Advances in Additive-Enhanced Magnesium Hydride for Hydrogen Storage *Progress in Natural Science: Materials International* 27 (1) 2017: pp. 41 – 49.
https://doi.org/10.1016/j.pnsc.2016.12.016
16. **Massalski, T.B.** Ed., Binary Alloy Phase Diagram, American Society for Metals, 1986.
17. **Yang, J.H., Yi, C.C., Xu, J.W., Ma, X.H.** Laser-induced Breakdown Spectroscopy Quantitative Analysis Method via Adaptive Analytical Line Selection and Relevance Vector Machine Regression Model *Spectrochimica Acta Part B* 107 2015: pp. 45 – 55.
https://doi.org/10.1016/j.sab.2015.02.014
18. **Atias-Adrian, I.C., Deorsola, F.A., Ortigoza-Villalba, G.A., DeBenedetti, B., Baricco, M.** Development of Nanostructured Mg_2Ni Alloys for Hydrogen Storage Applications *International Journal of Hydrogen Energy* 36 (13) 2011: pp. 7897 – 7901.
https://doi.org/10.1016/j.ijhydene.2011.01.047
19. **Yu, Y.N.** Metallography Principle (2nd Edition). Metallurgical Industry Press, 2013.
20. **Zhang, Y.H., Yuan, Z.M., Yang, T., Po, W.G., Hou, Z.H., Zhao, D.L.** Gaseous Hydrogen Storage Thermodynamics and Kinetics of RE–Mg–Ni-Based Alloys Prepared by Mechanical Milling *Journal of Central South University of Technology* 24 (4) 2017: pp. 773 – 781.
https://doi.org/10.1007/s11771-017-3479-8
21. **Sadhasivam, T., Kim, H.T., Jung, S.H., Roh, S.H., Jung, H.Y.** Dimensional Effects of Nanostructured Mg/MgH_2 for Hydrogen Storage Applications: A Review *Renewable and Sustainable Energy Reviews* 72 2017: pp. 523 – 534.
https://doi.org/10.1016/j.rser.2017.01.107